

Electronic structure and chemical bonding in semiconducting 3d transition-metal silicides CrSi₂, Mn₄Si₇, and β -FeSi₂

Motoharu Imai^{1*} and Masao Arai²

¹*Research Center for Electronic and Optical Materials, National Institute for Materials Science, Tsukuba, Ibaraki, 305-0047, Japan*

²*National Center for Basic Research on Materials, National Institute for Materials Science, Tsukuba, Ibaraki, 305-0044, Japan*

*E-mail: IMAI.Motoharu@nims.go.jp

The electronic properties and chemical bonding of semiconducting 3d transition-metal (TM) silicides—CrSi₂, Mn₄Si₇, and β -FeSi₂—were investigated using first-principles calculations. The density of states (DOS), orbital-projected DOS, and crystal orbital bond indices (COBIs) revealed that the electronic states of these silicides consisted of Si 3s states, bonding states of Si 3p and TM 3d orbitals, nonbonding states of TM 3d orbitals, antibonding states of Si 3p and TM 3d orbitals, and a bandgap (E_g) formed between the TM 3d nonbonding states and Si 3p-TM 3d antibonding states. The Löwdin charges and integrated COBI values indicate minimal charge transfer between the TM and Si atoms and suggest that the TM–Si interaction has a delocalized nature, similar to metallic bonding. Additionally, the E_g calculated using the generalized gradient approximation is comparable to the E_g determined experimentally for these silicides.

1. Introduction

Transition-metal (TM) silicides were extensively investigated as electrode materials for Si devices in the 1980s,^{1,2)} and an interaction diagram of silicides, as shown in Fig. 1, was proposed to clarify their electronic states.³⁾ According to this diagram, the electronic structure of TM silicides consists of Si 3s states, bonding and antibonding states between the Si 3p and TM d orbitals, and nonbonding states of the TM d orbitals. Semiconducting 3d-TM silicides such as CrSi₂, Mn₄Si₇, and β -FeSi₂ have been studied extensively as thermoelectric and optoelectric materials.⁴⁻⁸⁾ In the case of semiconducting silicides, the information where the bandgap (E_g) locates in the interaction diagram is useful for band engineering of semiconducting 3d-TM silicides. However, there are no reports on this topic.

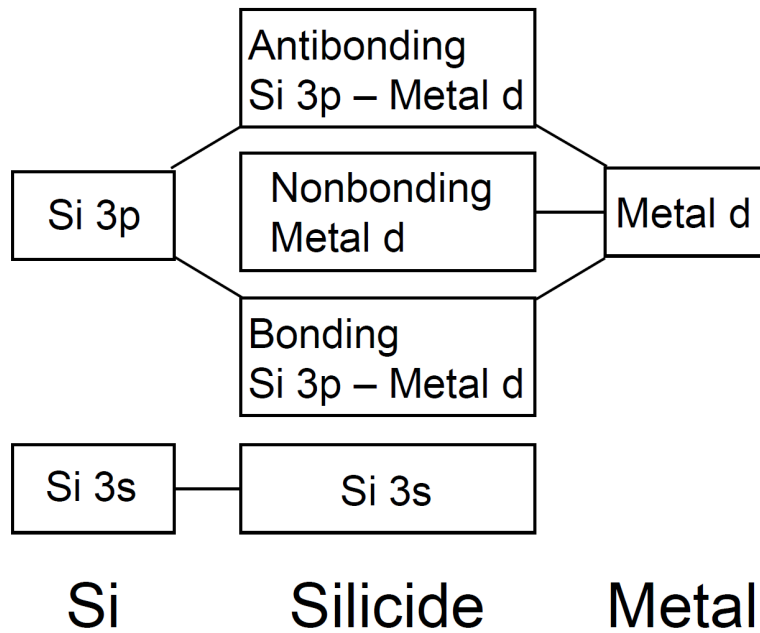


Fig. 1. Interaction diagram of TM silicides.³⁾

The electronic states and chemical-bonding characteristics of solids have been analyzed by calculating the density of states (DOS), orbital-projected density of states (pDOS), crystal orbital Hamilton population (COHP),^{9–13)} crystal orbital bonding indices (COBIs)^{14,15)} and Löwdin charges.¹⁶⁾ It is efficient to clarify E_g in the interaction diagram of TM silicides using the chemical-bonding information obtained from the calculations of the DOS, pDOS, and COBIs because pDOS reveals the contribution of each orbital to the electronic states, and the bonding, antibonding, and non-bonding states can be distinguished using their COBI values. Positive and negative COBI values correspond to bonding and antibonding electronic states, respectively. Furthermore, small COBI values correspond to nonbonding states.

In this study, the band structure, DOS, pDOS, COBI, and Löwdin charges were calculated for CrSi_2 , Mn_4Si_7 , and $\beta\text{-FeSi}_2$. On the basis of these results, we examined their chemical-bonding nature, along with the location of E_g in the interaction diagram in CrSi_2 , Mn_4Si_7 , and $\beta\text{-FeSi}_2$.

2. Methods

Electronic structures such as DOS and band structures were calculated using the projector augmented wave (PAW) method, as implemented in the Vienna Ab initio Simulation Package (VASP) code within the generalized gradient approximation (GGA) of Perdew, Burke, and Ernzerhof (PBE).^{17,18)} Spin-orbit coupling (SOC) was included self-consistently. The energy cutoff of 400 eV was used. The Γ -centered $15 \times 15 \times 8$, $9 \times 9 \times 3$, and $8 \times 8 \times 6$ k -meshes were used for CrSi_2 , Mn_4Si_7 , and $\beta\text{-FeSi}_2$, respectively. The electronic convergence criterion was set as 10^{-8} eV. The crystal structure was fully

optimized without the SOC using a criterion of $0.02 \text{ eV}\text{\AA}^{-1}$. The VASPKIT code was used to create the input files and analyze the output.¹⁹⁾

The COBI and Löwdin charges were calculated from the VASP output using the Local Orbital Basis Suite Towards Electronic Structure Reconstruction (LOBSTER) code.^{12–16)}

The PAW functions were projected onto local orbitals using the basis-function set pbeVaspFit2015 with the autorotate option.¹²⁾ The orbitals included were 3p, 3d, and 4s for the TM atoms and 3s and 3p for the Si atoms.

3. Results and discussion

3.1 Crystal structure

Table I presents details regarding the calculated crystal structures of (a) CrSi_2 , (b) Mn_4Si_7 , and (c) $\beta\text{-FeSi}_2$. The calculations reproduced the experimental lattice parameters reported in refs. 20–23 within an error of 1.5%, as shown in Table II, and the experimental internal parameters within an error of 2.1%.

Table I. Calculated crystal structure

(a) CrSi_2

Space group: $P6_222$ (No. 180)

Number of formula units in unit cell Z : 3

Lattice parameters (\AA): $a = 4.38040$, $c = 6.32897$

Site	Elements	Wyckoff position	x	y	z
Cr1	Cr	3d	1/2	0	1/2
Si1	Si	6j	0.166157	0.332314	1/2

(b) Mn_4Si_7

Space group: $P\text{-}4c2$ (No. 116)

Number of formula units in unit cell Z : 4

Lattice parameters (Å): $a = 5.46915$, $c = 17.27104$

Site	Elements	Wyckoff position	x	y	z
Mn1	Mn	2c	0	0	0
Mn2	Mn	4i	1/2	0	0.065034
Mn3	Mn	4h	1/2	1/2	0.130021
Mn4	Mn	4i	0	1/2	0.191643
Mn5	Mn	2a	0	0	1/4
Si1	Si	8j	0.155344	0.199730	0.112640
Si2	Si	8j	0.320660	0.841127	0.182430
Si3	Si	4e	0.333636	0.333636	1/4
Si4	Si	8j	0.346457	0.230434	0.961206

(c) β -FeSi₂

Space group: *Cmce* (No. 64)

Number of formula units in unit cell Z: 16

Lattice parameters (Å): $a = 9.86469$, $b = 7.7562$, $c = 7.7974$

Site	Elements	Wyckoff position	x	y	z
Fe1	Fe	8d	0.21644	0	0
Fe2	Fe	8f	1/2	0.30777	0.1873
Si1	Si	16g	0.12825	0.27375	0.05013
Si2	Si	16g	0.37351	0.04500	0.226735

Table II. Lattice parameters of CrSi₂, Mn₄Si₇, and β -FeSi₂ (Cal: calculation, Exp: experiment).²⁰⁻²³⁾

Silicide	Structure type	Crystal system	Lattice parameters (Å)			Remark	Ref.
			a	b	c		
CrSi ₂	CrSi ₂	Hexagonal	4.38039	-	6.32897	Cal	Present
			4.42758(7)	-	6.36805(11)	Exp	20
Mn ₄ Si ₇	Mn ₄ Si ₇	Tetragonal	5.46914	-	17.27104	Cal	Present
			5.510	-	17.418	Cal	21
			5.5259(5)	-	17.5156(8)	Exp	22
β -FeSi ₂	FeSi ₂	Orthorhombic	9.84694	7.75623	7.797395	Cal	Present
			9.863(7)	7.791(6)	7.833(6)	Exp	23

3.2 Band structure

3.2.1 CrSi₂

Fig. 2(a) shows the band structure of CrSi₂, in which the valence-band maximum (VBM) is set as 0 eV, indicating that CrSi₂ is an indirect-bandgap semiconductor with VBM and conduction-band minimum (CBM) located at the L and M points, respectively. Its E_g value is 0.368 eV (0.369 eV without SOC), which is consistent with a previously reported calculation result (0.35 eV).²⁴⁾ This calculated E_g value is comparable to the experimental one determined via optical absorption coefficient (α) measurement (0.35 eV).²⁵⁾

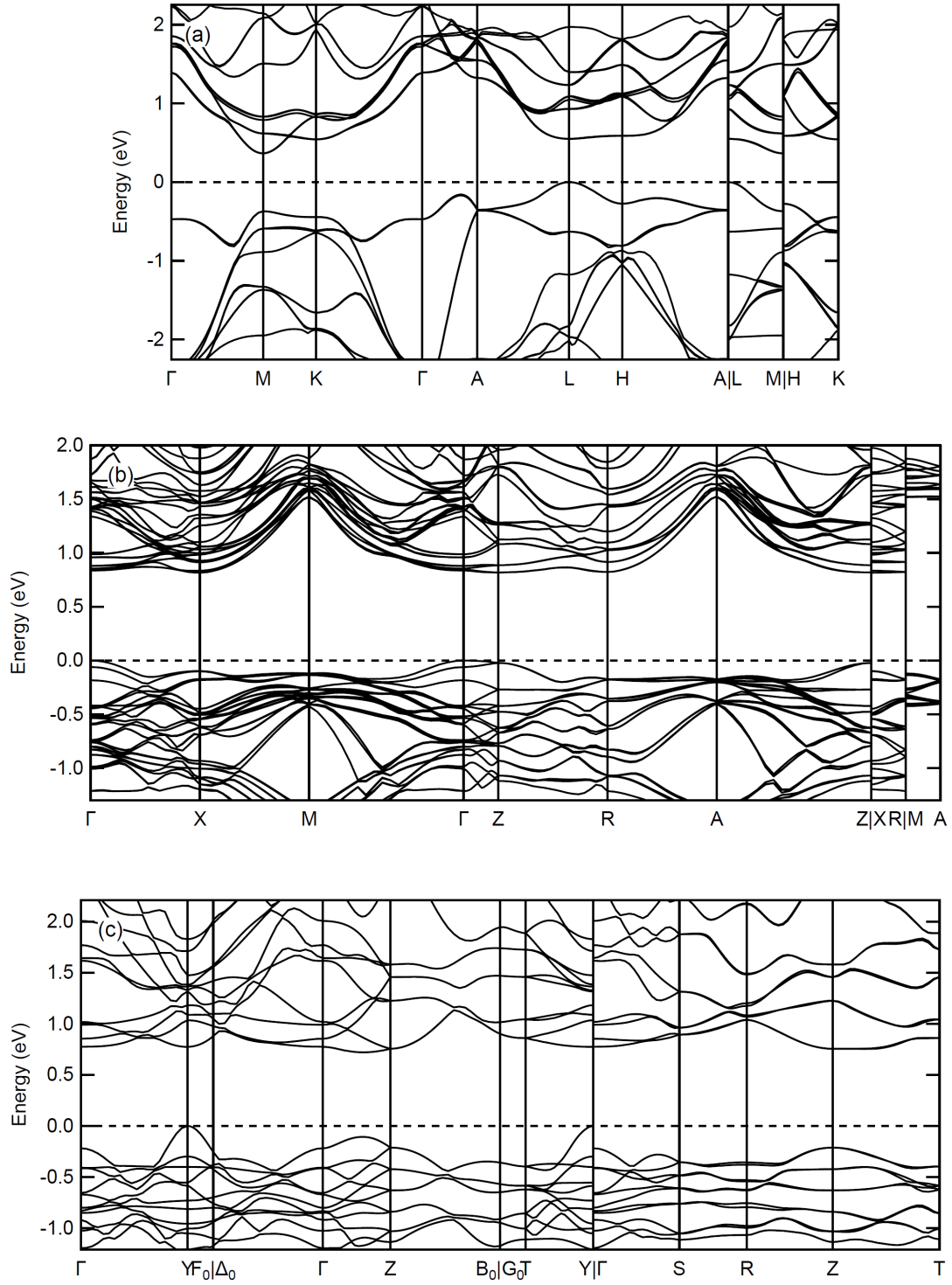


Fig. 2. Band structures of (a) CrSi₂, (b) Mn₄Si₇, and (c) β-FeSi₂.

3.2.2 Mn₄Si₇

The band structure of Mn₄Si₇ indicates that Mn₄Si₇ is an indirect-bandgap semiconductor with the VBM at the Γ point and CBM at the Z point, respectively, as shown in Fig. 2(b). The E_g value is 0.817 eV (0.818 without SOC), which slightly exceeds a previously reported

calculation result (0.769 eV).²¹⁾ As suggested by Migas, the E_g values for direct transitions at the Γ (0.840 eV) and Z (0.845 eV) points are close to the indirect- E_g value. The reported experimental E_g values range from 0.42 to 0.98 eV, as shown in Table III. In previous studies, α measurements using single-crystal and thin-film samples indicated that the Mn_4Si_7 phase had a direct bandgap of 0.78 eV.^{26,27)} Spectral ellipsometry of polycrystalline thin films with a preferred orientation relationship with the Si substrate revealed an indirect E_g of 0.4 eV.²⁸⁾ Recent α measurements using Mn_4Si_7 thin film samples containing a nearly strain-free Mn_4Si_7 phase had an E_g of 0.78 eV, and samples containing embedded strained Mn_4Si_7 precipitates exhibited an E_g of 0.93 eV.²⁹⁾ When the experimental E_g value is assumed to be 0.78 eV, the present calculated E_g value is consistent with the experimental value. The α for a direct transition is expected to be observed when the indirect- E_g value is close to the direct E_g value, because the magnitude of α for a direct transition is far larger than that for an indirect transition. This situation may occur in Mn_4Si_7 , because the indirect- E_g value is close to the direct E_g values at the Γ and Z points in the present calculation. This is plausibly why the experimentally observed α has photon-energy dependence for a direct transition although the calculations indicate that Mn_4Si_7 is an indirect- E_g semiconductor.

Table III. Bandgap E_g of Mn_4Si_7 . Experimental E_g values were obtained through optical absorption coefficient measurements (Cal: calculation, Exp: experiment).

E_g (eV)	Transition type	Remarks	Ref.
0.816	Indirect	Cal	Present
0.836	Direct at Γ point	Cal	Present
0.841	Direct at Z point	Cal	Present
0.769	Indirect	Cal	21
0.78	Direct	Exp	26,27
0.4	Indirect	Exp	28
0.78	Direct	Exp	29
0.92	Direct	Exp, strained	29

3.2.3 $\beta\text{-FeSi}_2$

$\beta\text{-FeSi}_2$ is an indirect- E_g semiconductor with the VBM at the Y point and CBM at a k point between the Γ and Z points (conventionally denoted as Λ^*), as shown in Fig. 2(c). The E_g value was 0.724 eV (0.723 wo SOC), which slightly exceeds the previously reported calculation result (0.68 eV).³⁰⁾ This calculated E_g value is comparable to the experimental one based on α measurements (0.814 eV).³¹⁾

Notably, the calculated E_g values for these three semiconducting silicides were comparable to the experimental E_g values, although the E_g values calculated using PBE-GGA underestimated the experimental values in many cases.³²⁾

3.3 DOS, COBI, and Löwdin charge

The left panels of Figs. 3 (a), (b), and (c) show the total DOS and pDOS of CrSi_2 , Mn_4Si_7 , and $\beta\text{-FeSi}_2$, respectively. The pDOS was calculated using LOBSTER code. The total DOS and pDOS of these three materials have the following common features: (1) the DOS located from -15 to -5 eV consists of Si 3s and Si 3p states, (2) the total DOS has two large peaks—P1 and P2—in the valence band (VB), (3) the peak at a higher energy P1 consists of TM 3d states and the peak at lower energy P2 consists of TM 3d and Si 3p states, and (4) the conduction band (CB) near bandgap mainly consists of TM 3d states. The energies of peaks P1 and P2 are presented in Table IV. Thus, the TM 3d states significantly contribute to the DOS of the VB and CB near E_g .

Table IV. Energies of two large peaks P1 and P2 in the DOS of the VB.

Silicide	Energy of P1 (eV)	Energy of P2 (eV)
CrSi_2	-0.65	-2.30
Mn_4Si_4	-0.20	-2.05
$\beta\text{-FeSi}_2$	-0.55	-1.60 eV

Figs. 4 (a), (b), and (c) illustrate the crystal structures of CrSi_2 , Mn_4Si_7 , and $\beta\text{-FeSi}_2$, respectively. Figs. 4 (d), (e), and (f) show the local structures around the transition-metal atoms highlighted by the orange circles in Figs. 4 (a)–(c). In these silicides, the nearest neighbors of the TM atoms are the Si atoms, and those of the Si atoms are the TM atoms. Therefore, we calculated the COBI of the TM–Si pairs with the shortest interatomic distances, as indicated by the red solid lines in the figure, and averaged them.

The right panels of Figs. 3 (a), (b), and (c) present the COBI for the Cr-Si bond of CrSi_2 , the Mn-Si bond of Mn_4Si_7 , and the Fe-Si bond of $\beta\text{-FeSi}_2$, respectively. The states with positive and negative COBI values are bonding and antibonding states, respectively. The states with small COBI values are nonbonding states. As mentioned previously, the pDOS of the TM 3d states exhibited two peaks in the VB. The ratio of COBI to DOS corresponding to the P1 peak in the DOS has a much smaller value than that to the P2 peak, indicating that this TM-3d state is a nonbonding state. The COBI corresponding to the P2 peak in the DOS has a large positive value, indicating that these TM pDOS states are the bonding states of the TM

3d-Si 3p states. The COBI that corresponds to the DOS in the CB has a large negative value, indicating that these states are antibonding states of the TM 3d-Si 3p states. Therefore, a bandgap exists between the TM-3d nonbonding states and TM 3d-Si 3p antibonding states, as shown in Fig. 5. These results provide a strategy for band engineering of semiconducting 3d-TM silicides: substituting Si atoms with other atoms affects the CB, whereas substituting TM atoms with other atoms affects both the VB and CB. This is helpful for tuning the electronic properties of semiconducting 3d-TM silicides.

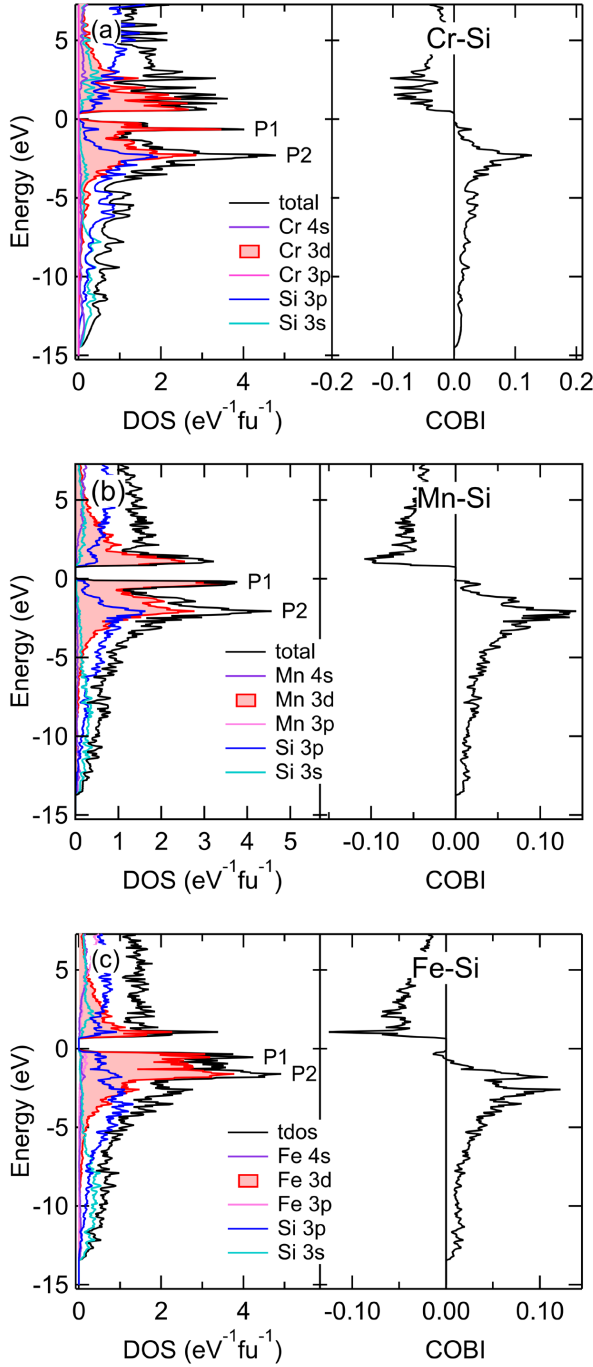


Fig. 3. Total DOS, p-DOS, and COBI of (a) CrSi₂, (b) Mn₄Si₇, and (c) β -FeSi₂.

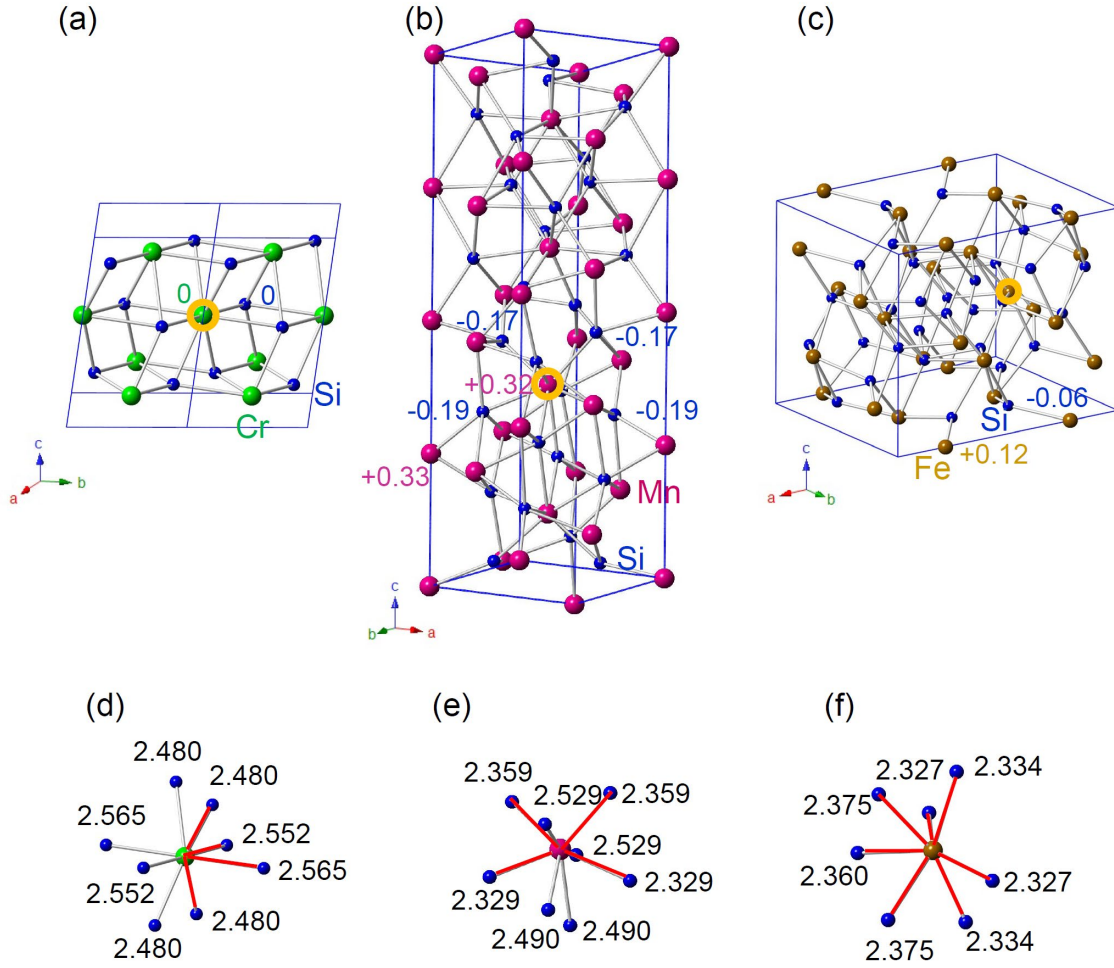


Fig. 4. Crystal structures of (a) CrSi₂, (b) Mn₄Si₇, and (c) β -FeSi₂. The blue lines depict the unit cell. The numbers in the figures are the Löwdin charges (in units of elementary charge e). (d)–(f) Local structures around the transition-metal atoms, highlighted by the orange circles in Figs. 4 (a)–(c). The red solid lines indicate TM–Si pairs whose COBI values were calculated. The numbers in the figures are interatomic distances (in units of Å).

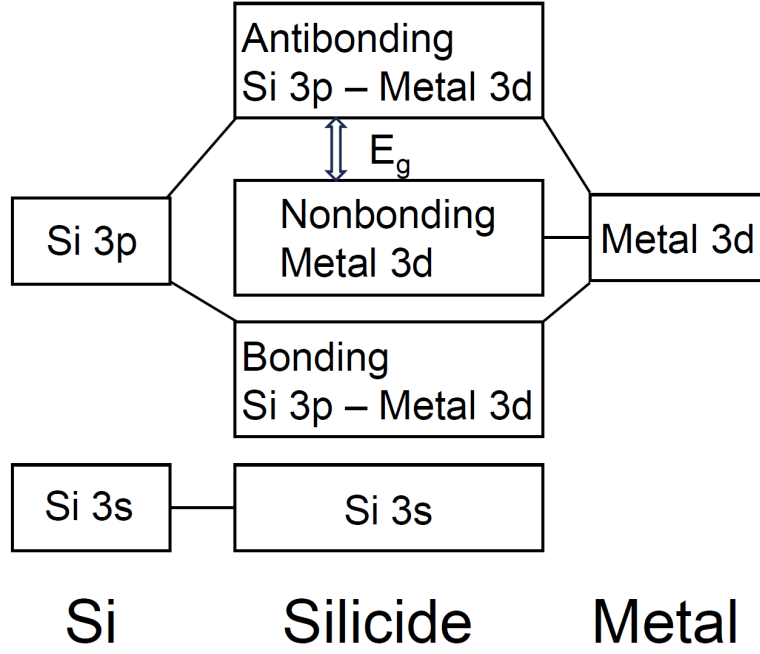


Fig. 5. Interaction diagram of semiconducting 3d-TM silicides CrSi_2 , Mn_4Si_7 , and $\beta\text{-FeSi}_2$.

The Löwdin charges and the integrated COBI (ICOBI) values for CrSi_2 , Mn_4Si_7 , and $\beta\text{-FeSi}_2$ are presented in Table V. The Löwdin charge of an atom is defined as the difference between the number of valence electrons and the gross orbital population, including all orbitals associated with the atom. The Löwdin charges suggest that no charge transfer occurs in CrSi_2 and that slight charge transfer occurs in Mn_4Si_7 and $\beta\text{-FeSi}_2$. The ICOBI value is the integrated value of COBI per bond up to the Fermi energy. Regarding two-center interactions, the ICOBI values tend to be >0.6 for purely covalent bonding, $0.2\text{--}0.6$ for delocalized interactions such as metallic bonding, and <0.2 for ionic bonding.¹⁵⁾ The calculated ICOBI values suggest that the three semiconducting silicides have delocalized metallic bonds, as in the case of MoSi_2 .¹⁵⁾

Table V. Löwdin charges and ICOBI for CrSi_2 , Mn_4Si_7 , and $\beta\text{-FeSi}_2$.

Silicide	Löwdin charge		ICOBI
	TM atom	Si atom	
CrSi_2	0e	0e	0.33
Mn_4Si_7	0.32e or 0.33e	−0.17e or 0.19e	0.43
$\beta\text{-FeSi}_2$	0.12e	−0.06e	0.36

4. Conclusion

The electronic properties and chemical bonding of the semiconducting 3d-TM disilicides CrSi_2 , Mn_4Si_7 , and $\beta\text{-FeSi}_2$ were investigated using first-principles calculations. We confirmed that the E_g calculated using the generalized gradient approximation was comparable to the E_g determined experimentally for these silicides. The calculated DOS, pDOS, and COBI revealed that the electronic states of these silicides consist of Si 3s states, bonding states of Si 3p and TM 3d, nonbonding states of TM 3d, and antibonding states of Si 3p and TM 3d and that E_g is formed between nonbonding states of TM 3d and antibonding states of Si 3p and TM 3d. The Löwdin charges and ICOBI suggest that the TM–Si interaction has a delocalized nature, such as metallic bonding with minimal charge transfer. The proposed interaction diagram provides the information necessary for band engineering of semiconducting 3d-TM silicides via substitution: substituting Si atoms with other atoms affects the CB, whereas substituting TM atoms with other atoms affects both the VB and CB. This information is helpful for the development of materials with enhanced properties.

Acknowledgments

The author thanks Y. Miyazaki of Tohoku University for inspiring us to construct the interaction diagram using the COHP and H. Ohtsuka of the National Institute of Material Science for instruction on the use of LOBSTER. Funding: This work was partially supported by Grants-in-Aid for Scientific Research (KAKENHI) [grant numbers JP22H00268 and JP21H01365] from the Japan Society for the Promotion of Science (JSPS).

References

- 1) S. P. Murarka, *Silicides for VLSI Applications* (Academic Press, New York, 1983).
- 2) M.-A. Nicolet and S. S. Lau, *Materials and Process Characterization* (Academic Press, New York, 1983), p. 329.
- 3) G. W. Rubloff, *Surf. Sci.* **132**, 268 (1983).
- 4) A. Nozariasbmarz, A. Agarwal, Z. A. Coutant, M. J. Hall, J. Liu, R. Liu, A. Malhotra, P. Norouzzadeh, M. C. Öztürk, V. P. Ramesh, Y. Sargolzaeiaval, F. Suarez, and D. Vashaee, *Jpn. J. Appl. Phys.* **56**, 05DA04 (2017).
- 5) A. T. Burkov, *Phys. Status Solidi A* **215**, 1800105 (2018).
- 6) T. Suemasu, K. Takakura, C. Li, Y. Ozawa, Y. Kumagai, and F. Hasegawa, *Thin Solid Films* **461**, 209 (2004).
- 7) Y. Maeda, *Thin Solid Films* **515**, 8118 (2007).

- 8) D. Z. Chi, *Thin Solid Films* **537**, 1 (2013).
- 9) R. Dronskowski and P. E. Bloechl, *J. Phys. Chem.* **97**, 8617 (1993).
- 10) V. L. Deringer, A. L. Tchougréeff, and R. Dronskowski, *J. Phys. Chem. A* **115**, 5461 (2011).
- 11) S. Maintz, V. L. Deringer, A. L. Tchougréeff, and R. Dronskowski, *J. Comput. Chem.* **34**, 2557 (2013).
- 12) S. Maintz, V. L. Deringer, A. L. Tchougréeff, and R. Dronskowski, *J. Comput. Chem.* **37**, 1030 (2016).
- 13) R. Nelson, C. Ertural, J. George, V. L. Deringer, G. Hautier, and R. Dronskowski, *J. Comput. Chem.* **41**, 1931 (2020).
- 14) P. C. Müller, C. Ertural, J. Hempelmann, and R. Dronskowski, *J. Phys. Chem. C* **125**, 7959 (2021).
- 15) L. S. Reitz, J. Hempelmann, P. C. Müller, R. Dronskowski, and S. Steinberg, *Chem. Mater.* **36**, 6791 (2024).
- 16) C. Ertural, S. Steinberg, and R. Dronskowski, *RSC Adv.* **9**, 29821 (2019).
- 17) G. Kresse and J. Furthmüller, *Phys. Rev. B Condens. Matter.* **54**, 11169 (1996).
- 18) G. Kresse and D. Joubert, *Phys. Rev. B* **59**, 1758 (1999).
- 19) V. Wang, N. Xu, J. C. Liu, G. Tang, and W. T. Geng, *Comput. Phys. Commun.* **267**, 108033 (2021).
- 20) K. Tanaka, K. Nawata, H. Inui, M. Yamaguchi, and M. Koiwa, *Intermetallics*. **9**, 603 (2001).
- 21) D. B. Migas, V. L. Shaposhnikov, A. B. Filonov, V. E. Borisenko, and N. N. Dorozhkin, *Phys. Rev. B.* **77**, 075205 (2008).
- 22) U. Gottlieb, A. Sulpice, B. Lambert-Andron, and O. Laborde, *J. Alloys Compd.* **361**, 13 (2003).
- 23) Y. Dusausoy, J. Protas, R. Wandji, and B. Roques, *Acta Crystallogr. B Struct. Crystallogr. Cryst. Chem.* **27**, 1209 (1971).
- 24) A. V. Krivosheeva, V. L. Shaposhnikov, and V. E. Borisenko, *Mater. Sci. Eng. B.* **101**, 309 (2003).
- 25) M. C. Bost and J.E. Mahan, *J. Appl. Phys.* **63**, 839 (1988).
- 26) M.C. Bost and J.E. Mahan, *J. Electron. Mater.* **16**, 389 (1987).
- 27) J. E. Mahan, *Thin Solid Films* **461**, 152 (2004).
- 28) M. Rebien, W. Henrion, H. Angermann, and S. Teichert, *Appl. Phys. Lett.* **81**, 649 (2002).
- 29) Y. Gao, G. S. Shao, Q. Li, Y. M. Xu, S. P. Wong, M. Y. Zhou, M. A. Lourenco, and K. P.

- Homewood, Jpn. J. Appl. Phys. **46**, 5777 (2007).
- 30) D. B. Migas, L. Miglio, W. Henrion, M. Rebien, F. Marabelli, B. A. Cook, V. L. Shaposhnikov, and V. E. Borisenko, Phys. Rev. B. **64**, 075208 (2001).
- 31) H. Udon, I. Kikuma, T. Okuno, Y. Masumoto, and H. Tajima, Appl. Phys. Lett. **85**, 1937 (2004).
- 32) J. Heyd, J. E. Peralta, G. E. Scuseria, and R. L. Martin, J. Chem. Phys. **123**, 174101 (2005).